UPCommons

Portal del coneixement obert de la UPC

Aquesta és una còpia de la versió *author's final draft* d'un article publicat a la revista *Journal of Fluids and Structures*.

URL d'aquest document a UPCommons E-prints:

Article publicat / *Published paper*:

Naseri, A., [et al.]. A semi-implicit coupling technique for fluid–structure interaction problems with strong added-mass effect. (2018) *Journal of Fluids and Structures*, vol. 80, p. 94-112. DOI: <10.1016/j.jfluidstructs.2018.03.012.>

A semi-implicit coupling technique for fluid-structure interaction problems with strong added-mass effect

Alireza Naseri*, Oriol Lehmkuhl, Ignacio Gonzalez, Eduard Bartrons, Carlos David Pérez-Segarra, Assensi Oliva

*Heat and Mass Transfer Technological Center (CTTC),
Universitat Politècnica de Catalunya-BarcelonaTech (UPC),
ESEIAAT, Colom 11, 08222 Terrassa (Barcelona), Spain*

Abstract

This paper is concerned with the numerical simulation of fluid-structure interaction problems involving an incompressible viscous flow and an elastic structure. A semi-implicit coupling technique is presented which strongly couples the added-mass term of the fluid (pressure stress) to the structure, while the remaining terms are only loosely coupled. A thorough numerical analysis is carried out to verify the accuracy of the proposed method by comparing its results to experimental data and other numerical results from the literature. The performance and accuracy of the proposed method are also compared against a fully implicit coupling technique. Numerical tests show that semi-implicit coupling significantly reduces the computational cost of the simulations without undermining either the stability or the accuracy of the results. The question of implicit or explicit coupling of the dynamic mesh step is addressed by evaluating its effect on the overall accuracy and performance of the semi-implicit method. The implicit coupling of the dynamic mesh step is found to slightly improve the accuracy, while significantly increasing the computational cost. Moreover a comparison is made on the performance of the semi-implicit method with different interface solvers.

Keywords:
fluid-structure interaction, numerical simulation, partitioned method, semi-implicit coupling

---

*Corresponding author.
    Email address: `anaseri@cttc.upc.edu` (Alireza Naseri)

1. Introduction

Fluid-structure interaction (FSI) refers to problems that deal with mutual interaction of fluid flow and a moving or deforming structure. On the one hand, fluid flow induces surface forces on the structure which make it move or deform. On the other hand, the movement of the solid boundary affects the fluid flow. A very wide range of applications is cited for FSI, ranging from civil engineering to biomechanics. An interesting example of FSI application in biomedical engineering is simulation of blood flow inside deformable vessels in human arterial system. The simulations may help improving the quality of artificial blood vessels and predicting the rupture of aneurysms during specific medical treatments or surgeries (e.g. [1, 2]). Another interesting application is predicting the flow-induced vibration on the submerged structures in offshore engineering (e.g. [3, 4]).

Broadly, two different approaches could be used to solve FSI problems, called monolithic and partitioned methods. In monolithic approach one uses a single solver to solve fluid and structural governing equations simultaneously. As the equations are solved together, the interaction between the domains is inherently taken into account. The main advantage of the monolithic approach is the elimination of the need for any further coupling technique at the fluid-structure interface, which reduces the complexity of the problem. However, this approach requires using the same numerical methods to discretize and solve the fluid and structural equations, while they are different in nature and have their own considerations. This may cause monolithic methods to be less efficient or reliable in some applications [5]. Another disadvantage of the monolithic approach is its inability to exploit the already-developed fluid and structural solvers. Therefore, it requires a large software development effort and usually results in a less modular solver [5, 6].

Partitioned methods, on the other hand, use separate solvers for fluid and structural equations and adopt a coupling scheme to account for the interaction of the domains. The coupling scheme determines the order and frequency in which the fluid and structural equations should be solved. It also determines the manner of communication and information exchange between the two solvers which is essentially restricted to the fluid-structure interface. Partitioned approach alleviates both disadvantages of the monolithic schemes. It allows using the most adapted numerical methods for each

sub-problem. These methods are previously tested and verified on diverse cases which greatly increases the reliability of the FSI simulations. It also enables the use of the previously developed solvers for fluid and structural equations which saves a large development effort and increases modularity of the software. However, partitioned approach introduces a new challenge to the problem, i.e. the coupling between the two solvers [5, 6].

Partitioned methods are further divided into explicit (or loosely coupled) and implicit (or strongly coupled) schemes. In an explicit coupling method, the fluid and structural equations are solved in sequence and only once at every time step. Consequently, explicit methods do not satisfy the exact coupling condition at the fluid-structure interface. The most basic explicit scheme is the conventional serial staggered method [7]. Implicit methods, in contrast, enforce the equilibrium condition at the interface by means of coupling iterations between the fluid and structural solvers at each time step. Fixed-point (Gauss-Seidel or Jacobi) iterations [5, 8] and Newton-based methods [9, 10, 11] are the most commonly used techniques to carry out the FSI coupling iterations. Vector extrapolation methods have also been used for this purpose [12].

Explicit methods work well for aeroelastic simulations and problems involving compressible flows [13, 14]. However they are unstable for a wide range of problems, especially ones with incompressible flow and low solid/fluid density ratios (values close to one). The instability is regardless of the time step size or discretization schemes for each domain. It is inherent to the coupling method and is often called "added-mass effect". The instability rises due to the fact that fluid forces in the explicit coupling depend upon a predicted displacement of the structure, rather than the correct one. As the structure moves, it has to accelerate the bulk of the fluid around it as well. Thus, part of the fluid acts as an extra mass in the structural dynamics system–given rise to the name added-mass effect. This effect is particularly strong when densities of the fluid and the structure are similar. For any loosely coupled method there is a density ratio limit that the method would suffer instability beyond it [15, 16]. While added-mass effect causes instability in the loosely coupled schemes, it deteriorates convergence of the strongly coupled methods. Thus, a FSI problem with strong added-mass effect is also challenging for implicit methods, as it requires many coupling iterations to converge at each time step [15, 16].

Implicit methods provide stable solution for FSI problems with strong added-mass effect, of which explicit methods are incapable. However, per-

3

forming several coupling iterations, i.e. solving the complete system of governing equations several times per time step, requires significantly higher computational resources. To alleviate this, Fernandez et al. [17] proposed a semi-implicit coupling technique in which they used a projection method to solve the fluid equations and only implicitly coupled the projection step to the structure. Therefore the pressure stress term of the fluid is strongly coupled to the structure. It is argued that the pressure stress term is the main contributor to the added-mass effect and coupling this term explicitly will cause numerical instability [15]. By implicit treatment of the added-mass term (pressure stress), the semi-implicit method maintains the favorable stability of the implicit schemes, while explicit treatment of the other terms helps avoiding excessive computational cost [17]. A very similar method was also proposed by Breuer et al. [18, 19] to solve FSI problems with turbulent flow. An analogous idea is present in the hybrid monolithic-partitioned method of Grétarsson et al. [20] for FSI problems with compressible flow. It strongly couples the fluid pressure and solid velocity by solving them implicitly in a monolithic manner, while the remaining terms are loosely coupled in a partitioned manner. Other semi-implicit methods are also reported in the literature which share the same basic idea, e.g. [21, 22].

Despite receiving attention from researchers, semi-implicit coupling technique is far from perfect. Many of the reported methods in the literature lack modularity and simplicity. Moreover most of the reported methods are only tested in a specific type of FSI problems and their robustness in dealing with different types of FSI problems is not evaluated. Besides, there are many unaddressed questions concerning different aspects of the semi-implicit coupling methods that require more work and attention. Some semi-implicit methods in the literature implicitly couple the dynamic mesh step of the fluid [18, 19], while others only explicitly couple it [17, 21, 22]. However, to the best of our knowledge, there has been no study that evaluates the effect of this modification on the overall performance and accuracy of the semi-implicit coupling method.

In this work, we follow a semi-implicit approach to develop an efficient coupling technique for FSI problems with strong added-mass effect. We also try to address some of the open questions concerning semi-implicit methods. The main improvements and advantages of the proposed method are as following.

- It is simple, modular and matrix-free. The method is developed with

4

the least possible mathematical and numerical complications. This results in a methodology which is easy to follow and simple to implement.

- It is robust. The method remains stable, accurate and efficient for a wide range of FSI problems, including ones with very large deformations. It is analyzed in three widely different test cases and has shown adequate stability and performance.

- It is computationally efficient. The proposed coupling technique along with the choices for numerical schemes and discretization, result in a fast and efficient overall methodology.

- It is suitable for simulating FSI problems with turbulent flow. The fluid solver and the coupling method are developed while special attention is paid to the particular considerations of turbulent flows.

A thorough analysis is carried out to verify the accuracy of the proposed method by comparing its results to experimental data as well as other numerical results from the literature. Numerical test cases are chosen to be very distinct in order to demonstrate the robustness of the method. Three test cases feature an internal flow contained by a deformable membrane, an external flow over a blunt body with rigid-body motion, and a cavity flow with a flexible bottom. Although the proposed method has been tested in turbulent FSI problems [23, 24], the attention is kept on laminar test cases, where the characteristics of the FSI method could be better highlighted.

The accuracy and computational cost of the method is compared against a fully implicit coupling technique. Moreover the effect of implicit or explicit coupling of the dynamic mesh step on the overall performance and accuracy of the semi-implicit method is evaluated. A modified version of the proposed method with implicitly coupled dynamic mesh step is also used for the numerical tests and its accuracy and performance are studied. Besides, both fixed-point and Newton-Krylov methods are used to solve the coupling interface problem and a comparison is made on their performance. Thus the main contributions of this paper could be highlighted as:

1. A simple, efficient and robust semi-implicit coupling method is proposed and its accuracy and good performance demonstrated through numerical tests.

2. The effect of implicit or explicit coupling of the dynamic mesh step on overall performance and accuracy of the semi-implicit scheme is evaluated.

3. Performance of fixed-point and Newton-Krylov interface solvers for semi-implicit coupling method is studied.

The rest of this paper is organized as follows. In section 2, the governing equations for each sub-domain as well as the coupling conditions on the interface are presented. The discretization methods and numerical schemes are also described in this section. In section 3, the proposed semi-implicit coupling technique is elaborated. Section 4 deals with the description of the methods used to solve the resulting interface problem. Results of the numerical tests and comparisons are provided in section 4, while section 5 summarizes and concludes the article.

2. Governing equations and numerical methods

In this section, the governing equations for each sub-problem domain and the coupling conditions on the interface are presented. The fluid and structural domains are referred to as $\Omega_f(t)$ and $\Omega_s(t)$ respectively, as they both vary in time. The interface of the domains is denoted by $\Gamma(t) = \Omega_f(t) \cap \Omega_s(t)$. An Arbitrary Lagrangian-Eulerian (ALE) formulation together with a conforming mesh technique [25, 26] is used to solve the fluid flow in a moving domain. A Lagrangian formulation is used for the structural equations.

2.1. Fluid equations

The unsteady flow of an incompressible viscous fluid is governed by the Navier-Stokes equations. An ALE formulation of these equations in a moving domain is given by

$$\nabla \cdot \mathbf{u} = \mathbf{0} \tag{1}$$

$$\frac{\partial \mathbf{u}}{\partial t} + \mathbf{c} \cdot \nabla \mathbf{u} = \frac{1}{\rho_f} \nabla \cdot \boldsymbol{\sigma}_f \tag{2}$$

where $\mathbf{u}$ is the fluid velocity and ρ_f the fluid density. Vector $\mathbf{c}$ is the ALE convective velocity $\mathbf{c} = \mathbf{u} - \mathbf{w}$, which is the fluid velocity relative to a domain moving with a velocity $\mathbf{w}$.

The stress tensor $\boldsymbol{\sigma}_f$ is defined for a Newtonian fluid as

$$\boldsymbol{\sigma}_f = -p\mathbf{I} + 2\mu_f\boldsymbol{\gamma} \tag{3}$$

where p is the fluid pressure, $\mathbf{I}$ the unit tensor, μ_f the dynamic viscosity of the fluid and $\boldsymbol{\gamma}$ the strain rate tensor given by

$$\boldsymbol{\gamma} = \frac{1}{2}(\nabla\mathbf{u} + \nabla\mathbf{u}^T) \tag{4}$$

2.2. Structural equations

The structural domain is governed by the nonlinear elastodynamics equation

$$\rho_s\frac{D^2\mathbf{d}}{Dt^2} = \nabla\cdot\boldsymbol{\sigma}_s \tag{5}$$

where $\mathbf{d}$ stands for the structural position with respect to the reference configuration, and the structural density is shown by ρ_s. The Cauchy stress tensor $\boldsymbol{\sigma}_s$ is related to the second Piola-Kirchhoff tensor $\mathbf{S}_s$ by

$$\mathbf{S}_s = J\mathbf{F}^{-1}\boldsymbol{\sigma}_s\mathbf{F}^T \tag{6}$$

where $\mathbf{F}$ is the deformation gradient $\mathbf{F} = \nabla\mathbf{d}$ and J is its determinant ($J = det(\mathbf{F})$).

The FSI coupling method is presented for a generic structural system at its full extent, however, simpler structural models are used for the numerical tests. The structural equations for each test case are explained in section 5.

2.3. Coupling conditions

The coupling conditions apply at the interface Γ and account for the interaction of the domains. They are derived from the kinematic and dynamic equilibrium between the domains, which yield to the following conditions on a non-slip type interface

$$\mathbf{u}_\Gamma = \frac{\partial\mathbf{d}_\Gamma}{\partial t} \tag{7}$$

$$\boldsymbol{\sigma}_s\cdot\mathbf{n}_\Gamma = \boldsymbol{\sigma}_f\cdot\mathbf{n}_\Gamma \tag{8}$$

for any point $\mathbf{x}\in\Gamma$, where $\mathbf{n}_\Gamma$ is the unit normal vector on the interface. Equation 7 represents equality of the velocity of the fluid and the structure on the interface to assure the kinematic equilibrium. Equation 8 represents equality of the traction on the interface for dynamic equilibrium.

2.4. Discretization and numerical methods

For fluid flow, a fractional-step projection method [27] along with an explicit time advancement is used to solve the velocity-pressure coupling of the momentum equation. This leads to a three step solution of the fluid governing equations from time step n to $n + 1$, with a time increment of Δt

$$\mathbf{u}^p = \mathbf{u}^n - \Delta t[(\mathbf{u}^n - \mathbf{w}^{n+1}).\nabla \mathbf{u}^n - \frac{\mu_f}{\rho_f}\Delta \mathbf{u}^n] \tag{9}$$

$$\frac{\Delta t}{\rho_{\mathrm{f}}}\Delta p^{\mathrm{n+1}} = \nabla.\mathbf{u}^{\mathrm{p}} \tag{10}$$

$$\mathbf{u}^{\mathrm{n+1}} = \mathbf{u}^{\mathrm{p}} - \frac{\Delta t}{\rho_{\mathrm{f}}}\nabla p^{\mathrm{n+1}} \tag{11}$$

for $\mathbf{x} \in \Omega_f^{n+1}$. For the sake of having a simple notation, a first-order Euler explicit time scheme is used for equation 9, but an extension to higher order schemes is straightforward. The method begins with evaluation of a predicted velocity, $\mathbf{u}^{\mathrm{p}}$, without considering the pressure gradient term (equation 9). A pressure field is then evaluated by solving a Poisson's equation (equation 10) that enforces the incompressibility condition at the velocity correction step (equation 11).

In this work, the fractional-step method is used not only for solving the fluid equations, but also as a framework for the overall FSI solution algorithm, making it fundamental to the proposed FSI coupling method.

A finite-volume method is used for the spatial discretization of the fluid equations on a collocated, unstructured mesh with second-order symmetry-preserving schemes. Symmetry-preserving schemes conserve the kinetic energy of the flow in discrete level [28]. Conservation of kinetic energy is extremely important while dealing with turbulent flows [29]. A conjugate gradient solver with a diagonal preconditioner is used to solve the Poisson's equation. A modern review and comparative study of advanced methods for solution of the Poisson's equation can be found in [30]. More details on the in-house flow solver code and the numerical methods can be found in [29, 31].

Structural equations are discretized in space using a finite-volume method along with a second-order central difference scheme. A second-order temporal scheme is used to discretize the second time derivative. More information on the numerical methods for the structural equations is provided in section 5 for each test case.

2.5. Mesh movement technique

Before equations 9-11 could be solved, the new fluid mesh in Ω_f^{n+1} and the surface velocities $\mathbf{w}^{n+1}$ are needed. A parallel moving mesh technique, based on radial basis function interpolation method [32], is used to move the fluid grid in accordance to the new location of the interface and update the discretized fluid domain.

The method uses values of scattered data, i.e. the known displacements of the nodes on the FSI interface, to evaluate an interpolated value in a cloud of points, i.e. the interior vertices of the fluid grid. Therefore, it does not need the connectivity of the mesh elements and can be applied to both structured and unstructured grids. The interpolated displacement $\delta\mathbf{r}$ at a point $\mathbf{x}$ is evaluated by:

$$\delta\mathbf{r}(\mathbf{x}) = \sum_{i=1}^{nv} \gamma_i \phi(||\mathbf{x} - \mathbf{x}_i||) + \mathbf{h}(\mathbf{x}) \tag{12}$$

where nv is the number of nodes on the FSI interface with known displacement and ϕ indicates the radial basis function. The radial basis function has been chosen to be the Wendland C^2 [33] since it preserves good quality of the dynamic mesh and allows to ignore the polynomial terms of the equation 12, $\mathbf{h}(\mathbf{x})$. The coefficients γ_i are determined by imposing the known solution on the interface

$$\delta\mathbf{r}(\mathbf{x}_i) = \delta\mathbf{d}(\mathbf{x}_i) \qquad i = 1, 2, ..., nv \tag{13}$$

for $\mathbf{x}_i \in \Gamma$, thus restricting the size of the system of equations to the number of known points nv.

Surface velocities are evaluated according to the so-called space conservation law (SCL). SCL states that the sum of the volumes swept by the surfaces of a control volume must be equal to the time rate of change of its volume v

$$\frac{\partial v}{\partial t} - \int_{cs} \mathbf{w} \cdot \mathrm{d}\mathbf{A} = 0 \tag{14}$$

where cs is the boundary of the control volume and $\mathbf{A}$ is the area vector pointing outward. For the discretized equations to be conservative in time, the surface velocities should satisfy SCL which guarantees no volume is lost while moving the grid. To satisfy the space conservation law exactly, surface velocities are evaluated by the volume swept by each surface $\mathbf{w}_{face} = \frac{\delta v}{A\delta t}.\mathbf{n}$

where A is the surface area, $\mathbf{n}$ surface normal vector, δt time step and δv the volume swept by the face (see Figure 1).
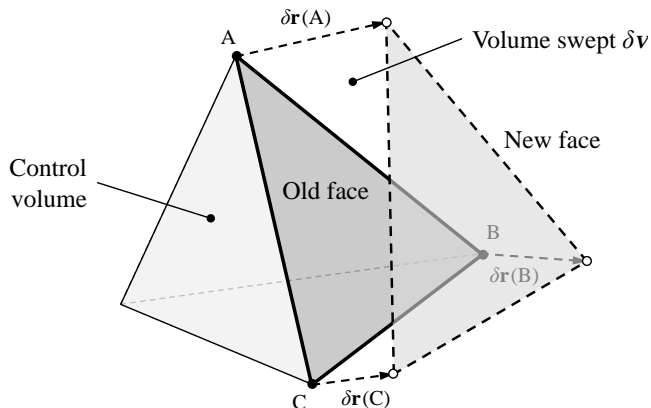

Figure 1: Volume swept by each face of an arbitrarily shaped polyhedral.

The process of moving the fluid mesh and evaluating the surface velocities at a new time step would be concisely denoted by the function $\mathbf{M}$ in the following sections

$$(\Omega_f^{n+1}, \mathbf{w}^{n+1}) = \mathbf{M}(\mathbf{d}_\Gamma^{n+1}) \tag{15}$$

More details concerning the mesh movement technique can be found in [32].

3. FSI coupling technique

A Dirichlet-Neumann (DN) decomposition of domains is used to solve the coupled FSI problem. In DN decomposition, fluid equations are solved for a known location of the interface and kinematic equilibrium (equation 7) is used as a Dirichlet boundary condition for fluid flow. Structural equations are solved for a known traction on the interface and are subject to Neumann boundary condition derived from dynamic equilibrium (equation 8). Thus the discrete fluid and structural equations can be represented as interface functions $\mathbf{F}$ and $\mathbf{S}$ so that

$$\boldsymbol{\sigma}_\Gamma = \mathbf{F}(\mathbf{d}_\Gamma) \tag{16}$$

$$\mathbf{d}_\Gamma = \mathbf{S}(\boldsymbol{\sigma}_\Gamma) \tag{17}$$

10

The discrete fluid function $\mathbf{F}$ includes equation 15 (mesh movement step) and equations 9-11 (Navier-Stokes equations). Given the current location of the interface, it moves the fluid mesh and solves the governing equations to obtain the fluid velocity and pressure fields. In particular, the fluid velocity and pressure on the interface are used to evaluate the fluid traction $\boldsymbol{\sigma}_\Gamma = \boldsymbol{\sigma}_f(p, \mathbf{u})_\Gamma \cdot \mathbf{n}_\Gamma$. The evaluated traction is then transferred to the structural function $\mathbf{S}$, which solves the governing equations of the structure to obtain the new location of the interface.

Therefore the discrete FSI equations can be represented as an interface problem of the form

$$\mathbf{S} \circ \mathbf{F}(\mathbf{d}_\Gamma) = \mathbf{d}_\Gamma \tag{18}$$

with vector $\mathbf{d}_\Gamma$ and functions $\mathbf{F}$ and $\mathbf{S}$, all in the same time step.

In an implicit FSI coupling method, equation 18 is solved iteratively at each time step. These methods show adequate stability but are computationally expensive because they require solving the fluid and structural equations several times at every time step. In most of applications, the fluid solver takes considerably more computational effort than the structural solver.

In this study we follow a semi-implicit approach in which only the pressure stress term of the fluid equations is implicitly coupled to the structure. Pressure stress term is the main contributor to the added-mass effect and must be coupled implicitly to avoid numerical instability [15, 17]. Using a fractional step method for fluid equations allows us to split the pressure stress term of the fluid (equation 10) and couple it implicitly to the structure. On the other hand, the rest of the fluid equations (Eqs. 15, 9 and 11) are only explicitly coupled. The complete algorithm of solving the FSI problem at time step $n + 1$ is as follows.

Semi-implicit FSI coupling method:
step 0: extrapolation of $\mathbf{d}_\Gamma$ from previous time steps:
$$\widetilde{\mathbf{d}}_\Gamma^{n+1} = 2.5\mathbf{d}_\Gamma^n - 2\mathbf{d}_\Gamma^{n-1} + 0.5\mathbf{d}_\Gamma^{n-2} \tag{19}$$

step 1: moving the fluid mesh (*explicitly coupled*):
$$(\Omega_f^{n+1}, \mathbf{w}^{n+1}) = \mathbf{M}(\widetilde{\mathbf{d}}_\Gamma^{n+1}) \tag{20}$$

step 2: ALE convection-diffusion equation (*explicitly coupled*):
$$\mathbf{u}^p = \mathbf{u}^n - \Delta t[(\mathbf{u}^n - \mathbf{w}^{n+1}).\nabla \mathbf{u}^n - \frac{\mu_f}{\rho_f}\Delta \mathbf{u}^n] \qquad \text{in } \Omega_f^{n+1} \tag{21}$$

11

step 3: pressure equation and structural solver (*implicitly coupled, solved iteratively*):

$$\mathbf{u}_\Gamma^p = \frac{\mathbf{d_\Gamma}^{n+1} - \mathbf{d}_\Gamma^n}{\Delta t} \qquad \text{on } \Gamma^{n+1} \tag{22}$$

$$\frac{\Delta t}{\rho_f} \Delta p^{n+1} = \nabla \cdot \mathbf{u}^p \qquad \text{in } \Omega_f^{n+1} \tag{23}$$

$$\boldsymbol{\sigma_\Gamma}^{n+1} = \boldsymbol{\sigma}_f(p^{n+1}, \mathbf{u}^p)_\Gamma \cdot \mathbf{n}_\Gamma \qquad \text{on } \Gamma^{n+1} \tag{24}$$

$$\mathbf{d_\Gamma}^{n+1} = \mathbf{S}(\boldsymbol{\sigma_\Gamma}^{n+1}) \qquad \text{on } \Gamma^{n+1} \tag{25}$$

step 4: velocity correction (*explicitly coupled*):

$$\mathbf{u}^{n+1} = \mathbf{u}^P - \frac{\Delta t}{\rho_f} \nabla p^{n+1} \qquad \text{in } \Omega_f^{n+1} \tag{26}$$

$$\mathbf{u}_\Gamma^{n+1} = \frac{\mathbf{d}_\Gamma^{n+1} - \mathbf{d}_\Gamma^n}{\Delta t} \qquad \text{on } \Gamma^{n+1} \tag{27}$$

With this semi-implicit coupling approach, the FSI interface problem (equation 18) is modified into:

$$\mathbf{S} \circ \mathbf{f}(\mathbf{d}_\Gamma) = \mathbf{d}_\Gamma \tag{28}$$

or

$$\mathbf{R}(\mathbf{d}_\Gamma) = \mathbf{S} \circ \mathbf{f}(\mathbf{d}_\Gamma) - \mathbf{d}_\Gamma = 0 \tag{29}$$

which stands for the step 3 of the above algorithm. In the new FSI equation, instead of the complete fluid solver function $\mathbf{F}$, only the pressure equation (denoted by $\mathbf{f}$) is coupled to the structure implicitly. Again, $\mathbf{d}_\Gamma$ and the functions $\mathbf{f}$ and $\mathbf{S}$ are in the same time step.

The proposed methodology is similar to the semi-implicit methods at [17, 19, 21, 22] in keeping the ALE convection-diffusion equation (steps 2) out of the FSI coupling loop. Avoiding to iterate this equation at every time step significantly reduces the computational cost of the simulations. Unlike the methods in [17, 19, 21, 22], the velocity correction step in the current method is outside the FSI coupling loop. FSI boundary condition is applied to the intermediate predicted velocity (rather than velocity itself) during the

coupling iterations (equation 22), thus avoiding to calculate the corrected velocity field at each iteration. When the FSI convergence is reached, the final velocity field is evaluated using the final pressure field and the final boundary displacement. Avoiding to iterate the velocity correction step further reduces the computational cost of the simulations.

Moreover, by applying the boundary condition on the predicted velocity, the shear stress term on the boundary (in equation 24) is evaluated using the updated values of velocity. For example, in [17, 21] the shear stress term is similarly evaluated using the predicted velocity field, however in their method the predicted velocity on the boundary is evaluated once at each time step and is not updated during the coupling iterations. It means methods in [17, 21] use a constant velocity vector on the boundary to evaluate the shear stress. In the present method we update the predicted velocity on the interface at every iteration and evaluate the fluid traction using current values of velocity.

Unlike [17, 21] an explicit temporal discretization scheme is used for the ALE convection-diffusion equation (equation 21). Explicit time-marching schemes are mostly preferred for their simplicity and lower computational cost, especially in the case of a turbulent flow where small time steps are inevitable. Keeping the convection-diffusion step out of the FSI loop provides the opportunity to use an explicit time-marching method which ought not to be missed.

In the semi-implicit coupling method proposed by Breuer [19], the mesh movement step is implicitly coupled to the structure. Since the ALE convection-diffusion step is out of the FSI loop, updating the fluid mesh and recalculating the geometrical derivatives at each coupling iteration only reflects in the Poisson's equation for pressure. On the other hand, moving the computational grid is an expensive step and including it in the coupling iterations would increase the computational cost of the method. This leads to the question of whether it is necessary and worthy to include the dynamic mesh step in the coupling iterations. No analysis to asses the extent of necessity and effect of this modification on the accuracy of the results is provided by Breuer et al. [19] or in other published works, to the best of our knowledge. In this work we have studied the effect of implicit coupling of the dynamic mesh step on the accuracy and performance of the semi-implicit method. For this purpose a modified version of the proposed method (referred to as semi-implicit-M in the rest of the text) is also used to solve the numerical test cases. The modified version is similar to the original one, except for the mesh movement

13

step (step 1) which is modified into $(\Omega_f^{n+1}, \mathbf{w}^{n+1}) = \mathbf{M}(\mathbf{d}_\Gamma^{n+1})$ and is repeated at every coupling iteration.

Finally, it should be noted that although the proposed coupling method requires a specific treatment of the fluid equations (using fractional-step method), it can be used with an arbitrary structural solver. Thus less attention is paid to the structural solver in this paper. However, the total performance improvement -with respect to a fully implicit coupling method- would indeed depend on the efficiency of the structural solver too.

4. Interface solvers

In this section we discuss the iterative methods to solve the nonlinear interface problem, arisen from the FSI coupling (equation 28 or 29). Fixed-point (FP) and Newton-Krylov methods are two family of solvers that have been widely used for FSI problems. In this study we have used both methods and compared their performance in a semi-implicit coupling.

4.1. Fixed-point solver

This is a class of iterative solvers that are popular mostly for their simplicity. They are very easy to implement and have proved to be efficient and robust in many problems. Jacobi and Gauss-Seidel iterations are the most basic and popular methods.

The fixed-point form of the interface problem is equation 28:

$$\mathbf{S} \circ \mathbf{f}(\mathbf{d}_\Gamma) = \mathbf{d}_\Gamma$$

A block Gauss-Seidel method is used in this study with the extrapolated value of $\mathbf{d}_\Gamma$ (equation 19) as the initial guess. Each iteration begins with solving the coupled system of equations

$$\widehat{\mathbf{d}_\Gamma}_{k+1} = \mathbf{S} \circ \mathbf{f}(\mathbf{d}_{\Gamma k}) \tag{30}$$

where k indicates the coupling iterations. The time step index is dropped for the sake of simplicity, as all the parameters are at the same time step. The interface residual is defined as

$$\mathbf{r}_{\Gamma k+1} = \widehat{\mathbf{d}_\Gamma}_{k+1} - \mathbf{d}_{\Gamma k} \tag{31}$$

and the line search step to update the solution is

$$\mathbf{d}_{\Gamma k+1} = \mathbf{d}_{\Gamma k} + \omega_k \mathbf{r}_{\Gamma k+1} \tag{32}$$

where ω_k is the relaxation factor. Relaxation is necessary for the stability of the scheme. It has been shown in several studies that unrelaxed Gauss-Seidel method either converges very slowly or does not converge at all for FSI problems involving an incompressible flow [5, 8]. Our numerical tests found the unrelaxed method unstable for the problems in hand. The relaxation factor is evaluated using Aitken's Δ^2 method. For a vector equation, ω_k could be obtained from:

$$\omega_k = -\omega_{k-1} \frac{\mathbf{r}_{\Gamma k}^T (\mathbf{r}_{\Gamma k+1} - \mathbf{r}_{\Gamma k})}{(\mathbf{r}_{\Gamma k+1} - \mathbf{r}_{\Gamma k})^T (\mathbf{r}_{\Gamma k+1} - \mathbf{r}_{\Gamma k})} \tag{33}$$

with $\omega_0 = 0.5$ used in this work for the first iteration.

FSI convergence is achieved at every time step when the ℓ_2 norm of the interface residual is small enough to meet the convergence criterion:

$$\frac{||\mathbf{r}_{\Gamma k}||_2}{||\mathbf{r}_{\Gamma 0}||_2} < \epsilon \tag{34}$$

with a predefined tolerance of ϵ ($\epsilon = 10^{-5}$ is used in the numerical tests).

4.2. Newton-Krylov solver

Newton-Krylov method consists of two levels of iterative solvers. The first level is a Newton's method to linearize the problem and the second level is a Krylov subspace method to solve the resulting linear system of equations (see [34] for a review). Newton-Krylov methods normally show a better performance than fixed-point methods since the FSI problem is highly nonlinear.

The interface problem is of the form of equation 29:

$$\mathbf{R}(\mathbf{d}_\Gamma) = \mathbf{S} \circ \mathbf{f}(\mathbf{d}_\Gamma) - \mathbf{d}_\Gamma = 0$$

Applying Newton's method we have

$$\mathbf{R}'(\mathbf{d}_{\Gamma k}) \Delta \mathbf{d}_{\Gamma k+1} = -\mathbf{R}(\mathbf{d}_{\Gamma k}) \tag{35}$$

$$\mathbf{d}_{\Gamma k+1} = \mathbf{d}_{\Gamma k} + \Delta \mathbf{d}_{\Gamma k+1} \tag{36}$$

15

where k is the coupling iteration index. The function $\mathbf{R}'$ denotes the interface Jacobian

$$\mathbf{R}'(\mathbf{d}_\Gamma) = \frac{d\mathbf{R}(\mathbf{d}_\Gamma)}{d\mathbf{d}_\Gamma} \tag{37}$$

Since the Jacobian matrix of the coupled system of fluid-structure equations is not easily accessible, a matrix-free Krylov subspace solver is used to solve the Newton's equation (equation 35). The advantage of the Krylov solvers is that they only need the product of the Jacobian matrix and a vector, rather than the Jacobian matrix itself. A first order Taylor series expansion is used to approximate the product of the Jacobian matrix and an arbitrary vector $\mathbf{v}$

$$\mathbf{R}'(\mathbf{d}_{\Gamma k})\mathbf{v} = \frac{\mathbf{R}(\mathbf{d}_{\Gamma k} + \delta\mathbf{v}) - \mathbf{R}(\mathbf{d}_{\Gamma k})}{\delta} \tag{38}$$

with δ evaluated as $\delta = \lambda(\lambda + \frac{||\mathbf{d}_{\Gamma k}||_2}{||\mathbf{R}(\mathbf{d}_{\Gamma k})||_2})$, where λ is a sufficiently small number ($\lambda = 10^{-4}$ in this work), as suggested in [8]. Other approaches to choose δ could be found in [34].

An unpreconditioned GMRES solver [35] is used in this study as the Krylov solver. GMRES is chosen for its favorable convergence and robustness, considering that the FSI problem is highly nonlinear. We have also tried the BiCGSTAB method [36] as the Krylov solver but it showed convergence problems in some of the numerical tests.

FSI convergence criterion for Newton-Krylov solver is identical to that of the fixed-point method (equation 34 with a tolerance $\epsilon = 10^{-5}$). However, its performance also depends on the tolerance for convergence of its inner Krylov solver ϵ_k. In this work we set a high tolerance for the Krylov solver so that Newton's equation is solved with a rough accuracy. Therefore, Krylov solver takes less iterations to solve each Newton step, but more Newton steps are required to reach FSI convergence. We have seen that the overall efficiency of the method is improved in this arrangement, comparing to the case of an accurate Krylov solver. In order to optimize the performance of the method, ϵ_k is evaluated dynamically at every Newton step by

$$\epsilon_k = \gamma \left(\frac{||\mathbf{R}(\mathbf{d}_{\Gamma k})||_2}{||\mathbf{R}(\mathbf{d}_{\Gamma k-1})||_2} \right)^\alpha \tag{39}$$

16

with $\gamma = 1$ and $\alpha = (1 + \sqrt{5})/2$ as suggested in [37]. A minimum limit, $\epsilon_{k(min)} = 10^{-3}$, is set to avoid smaller values.

5. Numerical tests

Three numerical test cases are studied to demonstrate the accuracy, stability and the computational efficiency of the proposed methodology. The test cases are widely distinct and are chosen to demonstrate the robustness of the method in dealing with different types of FSI problems. All test cases are previously studied in the literature and represent important and practical FSI problems. The first test case is a bio-inspired FSI problem of incompressible flow inside a deformable vessel. The problem features a very low solid/fluid density ratio, which signifies a very strong added-mass effect. This test case is very challenging in terms of stability and convergence and is used here to demonstrate the stability of the method and its higher efficiency. The second test case is the vortex-induced vibration of an elastically mounted cylinder in low Reynolds number external flow. Unlike the other two test cases, the structure is not a thin-walled deformable membrane, but a rigid body moving inside the flow field. The added-mass effect is smaller for this test case but it features larger displacements. Moreover, there are available experimental data for this case that serve to validate the method. The third test case is a driven cavity with a flexible bottom. This test case features very large deformations and is used to further demonstrate the capability of the method to deal with large displacements of the solid boundary.

5.1. 3D flow inside a deformable tube

This benchmark problem was proposed by [38] and studied, among others, by [8, 10, 17]. The problem is a 3D flow inside a straight tube with a deformable wall, motivated by the type of problems encountered in hemodynamics. The tube has a length of $l = 0.05$m, an inner radius of $R_0 = 0.005$m and a wall thickness of $h = 0.001$m. The fluid density and viscosity are $\rho_f = 1000$kg/m^3 and $\mu_f = 0.003$Pa$\cdot$s, respectively. The structural density is $\rho_s = 1200$kg/m^3, the Young modulus $E = 3 \times 10^5$N/m^2, the Poisson ratio $\xi = 0.3$, and the Timoshenko factor is $k = 5/6$. The density ratio is very small $(\rho_s/\rho_f = 1.2)$ which means there is a very strong added-mass effect present.

A simplified form of the Navier equations for vascular walls [39] is used to model the deformable structure. The model is derived from the theory

17

of linear elasticity, considering only the radial deformation of the vessel and neglecting the shear stress terms in the structure. The governing equation of the structure reads

$$\rho_s h \frac{\partial^2 \mathbf{d}}{\partial t^2} - kGh \frac{\partial^2 \mathbf{d}}{\partial z^2} + \frac{Eh}{1 - \xi^2} \frac{\mathbf{d}}{R_0^2} = \boldsymbol{\sigma}_\Gamma \tag{40}$$

where $\mathbf{d} = [d_1, 0, 0]^T$ and $\boldsymbol{\sigma}_\Gamma = [\sigma_1, 0, 0]^T$ in a cylindrical coordinate (r, θ, z). A detailed description of the model could be found in [39, 40].

The tube wall is considered a thin structure so a 2D grid in the cylindrical coordinate is used for the structure. The structural grid nodes match the fluid mesh on the interface so there is no need for interpolation of parameters between the domains. Structural equation is discretized in space using a finite-volume method along with a second-order central difference scheme. An implicit second-order finite difference scheme is used to discretize the second time derivative.

The tube is clamped at both ends and the fluid is initially at rest. An overpressure of 1333.2Pa is applied at the tube inlet during a period of 0.003s and a constant pressure of 0Pa afterwards. Pressure at the outlet is 0Pa during the whole simulation. Neumann boundary condition is used for velocity at both inlet and outlet boundaries. Simulations are carried out during 0.01s with a constant time step of $\Delta t = 10^{-4} s$.

Propagation of the pressure wave with a finite velocity is observed inside the tube. Figure 2 shows the pressure contour plots at three different time instants: t=0.0025, 0.005 and 0.0075 s. Deformation of the tube wall is magnified by a factor of 10 to be visible more clearly.

The mesh-independency of the results is assessed by using three different grids to solve the problem. Two parameters are used to evaluate the accuracy, namely the inner radius of the mid-point of the tube at $t = 0.005s$, and the outlet mass flow rate at $t = 0.009s$. The two parameters are chosen because they represent the physics of the problem. The timing is also chosen to represent the instants of interest, i.e. the instants when the peak of the wave is in the area of the target parameter. Table 1 contains the information of the grids and results of the simulation.

As noticeable in Table 1, results obtained by mesh M2 and M3 are very similar. The M1 mesh gives good results for mid-point radius but the outlet mass flow is about 4% different. Mesh M2 is used to carry out the rest of the simulations for the sake of both accuracy and computational cost.
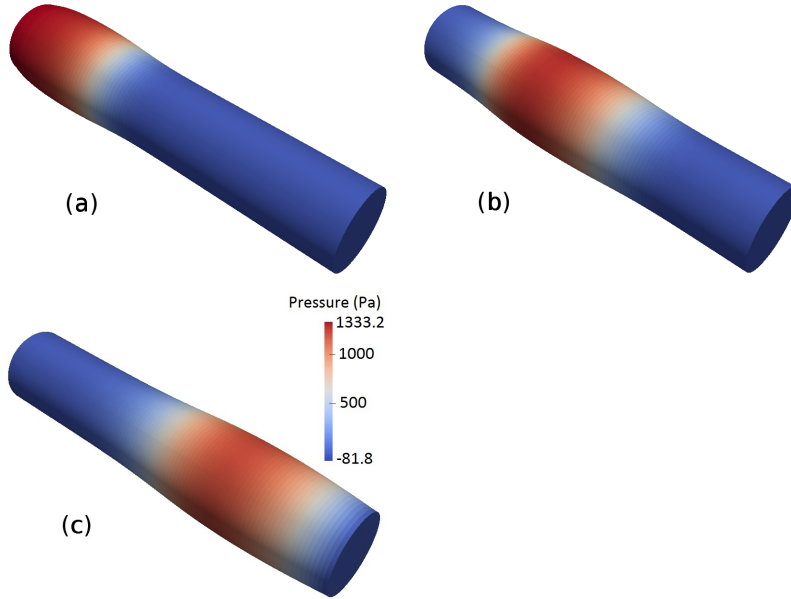
Figure 2: Pressure wave propagation inside the deformable vessel: (a) t=0.0025s, (b) t=0.005s and (c) t=0.0075s.

In order to verify the accuracy of the proposed method, the problem was also solved using a fully implicit coupling technique to generate reference results. For the implicit coupling, equation 18 is solved iteratively using the interface solvers described in section 4. It means all fluid terms and the dynamic mesh step are strongly coupled to the structure via coupling iterations. Table 2 represents the results obtained by the implicit, semi-implicit and semi-implicit-M coupling methods. Same parameters are used to evaluate the accuracy of the methods.

Results in Table 2 demonstrate the adequate accuracy of the proposed semi-implicit coupling method. The maximum error in mid-point radius is less than 0.1% while outlet mass flow rate has an error of 1.1% (with respect to results of the implicit method). The level of the error is very low which suggests the semi-implicit coupling method does not degrade the accuracy of the solution, compared to a fully implicit method. Including the mesh movement step in the coupling iterations (semi-implicit-M method) further reduces the error to under 0.4%.

Moreover, Figure 3 compares the transient results obtained by the semi-

Table 1: Mesh-independency of the results for deformable tube test case.

| Mesh name | Grid size | | mid-point radius | outlet mass flow |
	Fluid	Structure	t=0.005s (mm)	t=0.009s (g/s)
M1	3742	1267	5.01	24.50
M2	8776	2760	5.05	25.38
M3	19156	4450	5.05	25.49

Table 2: Comparison of the accuracy of the implicit and semi-implicit methods for deformable tube test case.

Coupling method	mid-point radius t=0.005s (mm)	outlet mass flow t=0.009s (g/s)
Implicit	5.05	25.67
Semi-implicit	5.05	25.38
Semi-implicit-M	5.05	25.57

implicit method against those of the fully implicit scheme. The picture in the left shows the radius at the mid-point of the tube while the picture in the right depicts the mass flow rate at the outlet, during the simulation time. Results of the semi-implicit method agree very well with those of implicit method at every time step which further verifies the accuracy of the proposed method.

Table 3 compares the performance of the implicit and semi-implicit coupling methods. The performance criteria are the average number of coupling iterations at each time step and the overall CPU time of the simulations. CPU times are presented in non-dimensional form. They are normalized by the smallest value, which is that of the semi-implicit method. All three coupling methods have been used with the same interface solver (FP-Aitken). Simulations were carried out on a machine with two Quad-Core AMD Opteron 2376 CPUs (8 cores in total) and 16GB of RAM. The machine was used exclusively for the solution of each case with identical conditions in order to attain comparable CPU times.

Data in Table 3 demonstrate the significantly lower computational cost of the proposed semi-implicit coupling method with respect to implicit coupling technique. Comparing the total CPU times of the implicit and semi-implicit
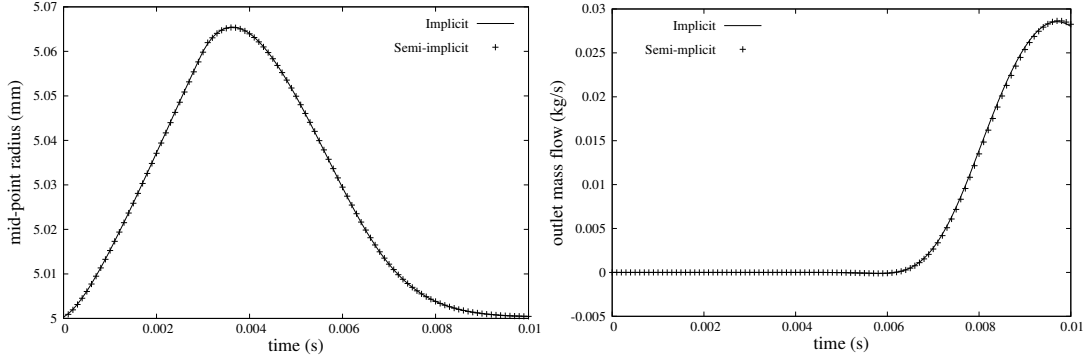
Figure 3: Comparison of the transient results obtained by implicit and semi-implicit coupling methods, left: inner radius of the mid-point of the tube, right: outlet mass flow rate.

Table 3: Performance comparison of implicit and semi-implicit coupling methods in deformable tube test case.

Coupling technique	Average No. of coupling iterations	Normalized CPU time
Implicit	39.7	12.9
Semi-implicit	36.3	1.0
Semi-implicit-M	38.5	11.2

methods shows that semi-implicit coupling reduces the computational time by 92%. This significant reduction in CPU time is because the semi-implicit method avoids iterating the expensive steps of the solution procedure described in section 3.

The required CPU time for the semi-implicit-M method is significantly higher. It takes 11.2 times more computational time than the semi-implicit method, and it is only 13% faster than the implicit coupling scheme. Including the mesh movement step in the coupling iterations is the reason for such a high computational cost of the modified semi-implicit method. Clearly the relative CPU time of this method highly depends on the performance of the dynamic mesh technique. With a simple and fast mesh movement tool, its performance would be closer to the semi-implicit method. However, in many applications the quality of the mesh near the solid surfaces is of utmost im-

portance. Hence an advanced mesh movement technique which guarantees the high quality of the mesh elements in vicinity of the moving boundary is indispensable. Such advanced mesh movement techniques (like the method used in this work) are normally very costly, which remarkably increases the computational cost of the simulations.

Based on results in Table 2 and 3, including the mesh movement step in the coupling iterations only slightly improves the accuracy of the results, while significantly increasing the computational cost. As discussed in section 3, updating the fluid mesh in the semi-implicit method only affects the coefficients of the Poisson's equation for pressure. We have seen in the present numerical test that the change in the pressure field due to updating the mesh, and the subsequent changes in the location of the interface and other flow parameters, are marginal. This could be partly due to the relatively small deformation of the structure and small time step size in the current test case. In the following subsections we would study this effect in FSI problems with larger displacement of the interface boundary.

It is worth to note that the semi-implicit method reduces the computational cost of each coupling iteration but does not particularly affect the number of coupling iterations required for convergence. The average number of coupling iterations for implicit and semi-implicit techniques are very similar (Table 3). The number of iterations to reach convergence at each time step is mostly affected by the iterative solver that is used to carry out the coupling iterations. Two basically different interface solvers were used to solve the coupled interface problem, as explained in section 4. The performance of these solvers are reflected in Table 4, using four criteria. The first criterion is the average number of coupling iterations at each time step. The second criterion represents the number of times that the coupled equations $(\mathbf{S} \circ \mathbf{f}(\mathbf{d}_\Gamma))$ are solved at each coupling iteration. This number is essentially equal to 1 for the fixed-point solver but is higher for the Newton-Krylov method, because it undergoes an inner loop inside every coupling iteration. The third criterion is the number of times that the coupled equations are solved at each time step (the product of the first and the second criteria). The last criterion is the overall CPU time of the simulations, normalized by the smallest value which is that of the Newton-Krylov method.

It is seen in the data of Table 4 that the nonlinear Newton-Krylov method outperforms the fixed-point method. It reduces the average number of solving the coupled equations by almost half with respect to FP-Aitken method (third criterion in Table 4). Comparing the CPU times, FP-Aitken takes 27%

Table 4: Performance comparison of different interface solvers for semi-implicit coupling method in deformable tube test case.

Interface solver	Average No. of coupling iterations	No. of $\mathbf{S} \circ \mathbf{f}(\mathbf{d}_\Gamma)$ solutions per coupling iteration	Average No. of $\mathbf{S} \circ \mathbf{f}(\mathbf{d}_\Gamma)$ solutions per time step	Normalized CPU time
FP-Aitken	36.3	1	36.3	1.27
Newton-Krylov	4.0	4.6 (average)	18.4	1.00

more computational time than the Newton-Krylov solver. It should be noted that comparing the number of coupling iterations for these two methods is not appropriate because Newton-Krylov method takes considerably more computational time per coupling iteration.

The current test case is a FSI problem with a very strong added-mass effect that takes many coupling iterations to satisfy the equilibrium condition on the interface. The reduction in computational time by using the Newton-Krylov method is tangible. It should be mentioned that although Newton-Krylov method outperforms the FP-Aitken, it introduces more complexity to the problem due to evaluation of the Jacobian. It is also worth to mention that an unpreconditioned Krylov solver has been used to solve the Newton's equation in this work. Using a preconditioner normally boosts the performance of a Krylov solver, however, designing a preconditioner in FSI applications is not straightforward due to the unavailability of the Jacobian matrix. In the next subsection we will compare the performance of both interface solvers in a FSI problem that is far less demanding in terms of required number of coupling iterations.

5.2. Vortex-induced vibration of a circular cylinder

In this test case we solve the external flow over an elastically mounted circular cylinder and study the vibrations induced by the flow vortices. Vortex-induced vibration (VIV) is an important class of FSI problems with a wide range of applications in aerodynamics and offshore engineering.

The cylinder is elastically mounted and oscillates due to the fluctuating fluid forces that are originated from vortex shedding phenomenon. In a certain range of Reynolds number, the vortex shedding frequency changes to

match the natural structural frequency of the cylinder motion. This range of Reynolds number is called *lock-in* region since the vortex shedding no longer occurs in the Strouhal frequency, but in the natural structural frequency of the cylinder.

In order to validate the proposed method, a series of VIV simulations in low Reynolds numbers was carried out to numerically reproduce the experimental results of Anagnostopoulos and Bearman [41]. The cylinder was constrained to oscillate transversely only, as per the experiments. A sketch of the domain and problem setup is shown in Figure 4. The domain size is chosen based on previous experience on flow over a fixed cylinder and guidance from other VIV studies in the literature. A uniform flow with a velocity U_∞ enters the domain at the inlet boundary. Pressure is set to zero at the outlet while a Neumann boundary condition is used for the velocity. For the sake of computational efficiency, the dynamic mesh and ALE formulation is restricted to a zone of 5D distance from the center of the cylinder. The computational grid in the rest of the domain is fixed (not moving) and an Eulerian formulation is applied.
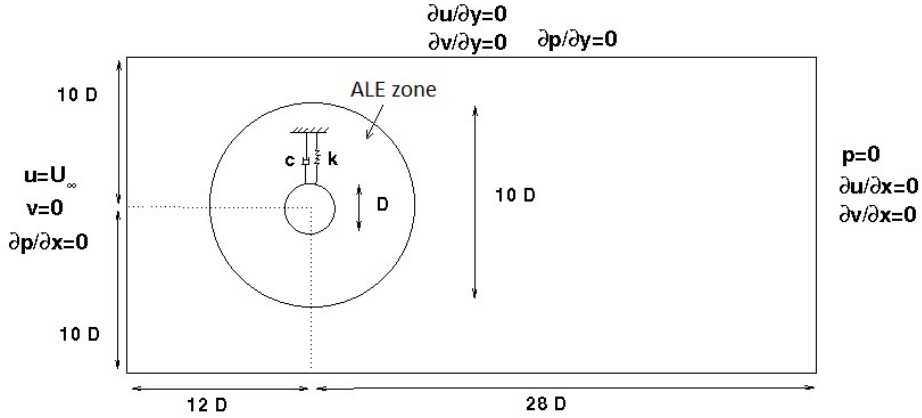

Figure 4: Schematic view of the domain and problem setup for the VIV test case.

The equation of motion of the cylinder is described by

$$m\frac{\partial^2 \mathbf{d}}{\partial t^2} + c\frac{\partial \mathbf{d}}{\partial t} + k\mathbf{d} = \mathbf{q}(t) \tag{41}$$

where $\mathbf{d} = [0, y, 0]^T$, y being the vertical location of the center of the cylinder.

The oscillation system parameters, m stands for the cylinder mass, c the damping coefficient and k is the spring stiffness. The vertical component of the time-variant fluid force (pressure and shear forces) on the cylinder is shown by $L(t)$ so that $\mathbf{q}(t) = [0, L(t), 0]^T$. The cylinder has a natural frequency of $f_n = \frac{1}{2\pi}\sqrt{\frac{k}{m}}$. Table 5 shows the definition of the relevant non-dimensional numbers and their values. All non-dimensional numbers equal those of the experiments [41]. The Reynolds number varies between 90 to 140 and the associated reduced velocity between 5.01 to 7.80. The variable l in the definition of mass ratio is the length of the cylinder.

Table 5: Relevant non-dimensional numbers of the VIV problem.

Name	Definition	Value
Reynolds (Re)	$\rho_f U_\infty D/\mu_f$	90-140
Reduced velocity (U_r)	$U_\infty/(f_n D)$	5.01-7.80
Mass ratio	$\rho_f D^2 l/2m$	0.00427
Damping ratio	$c/2\sqrt{km}$	0.0012

To evaluate the mesh-independency of the results, three fluid grids are used to solve the problem at Re=100. Table 6 contains the information of the grids and compares their results. Parameters in the table are mesh size, amplitude of the vibrations $A^* = y_{max}/D$, vortex shedding frequency f divided by natural frequency of the cylinder f_n, and the drag coefficient of the cylinder C_d.

Table 6: mesh-independency of VIV results at Re=100.

Mesh name	No. of control volumes	A^*	f/f_n	C_d
M1	7195	0.394	0.967	1.40
M2	13685	0.418	0.988	1.59
M3	27091	0.423	0.992	1.61

As results in Table 6 demonstrate, the grids M2 and M3 yield very similar results. Considering both accuracy and computational cost, mesh M2 is used for the rest of the simulations. Figure 5 shows the mesh M2 at its

original condition (Figure 5-a) and when the cylinder is at the peak of its oscillation (displacement of 0.42D for Re=100), in Figure 5-b. A closer zoom is also provided to better see the mesh elements around the cylinder. It could be seen in the figure that the mesh movement technique has preserved the quality of the mesh, particularly in the vicinity of the solid boundary.
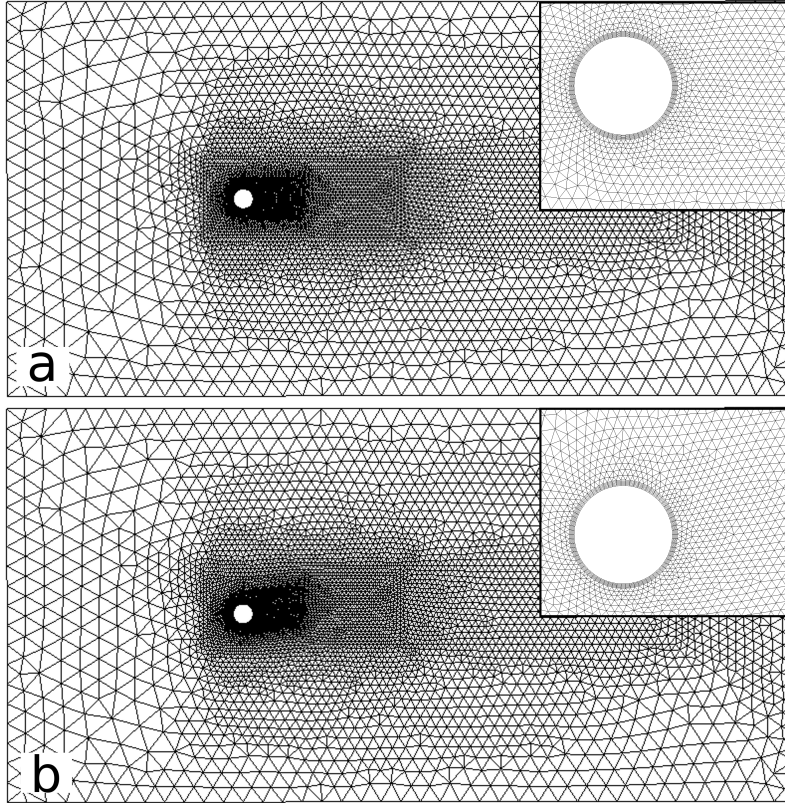

Figure 5: Computational grid around the cylinder, a: original mesh when y=0, b: moved mesh when y=-0.42D.

Figure 6 shows the results of the VIV simulations and compares them against experimental data [41] and other numerical results [42, 43, 22]. Plotted data are the amplitude of cylinder vibration and vortex shedding frequency for different Reynolds numbers.

As seen in the Figure 6, the method has captured the lock-in phenomenon. For Reynolds numbers $Re < 95$ and $Re > 115$ the vortex shedding occurs at the Strouhal frequency, the cylinder is *unlocked* and the amplitude of the oscillations is small. For $95 < Re < 115$ the cylinder is *locked-in* and the
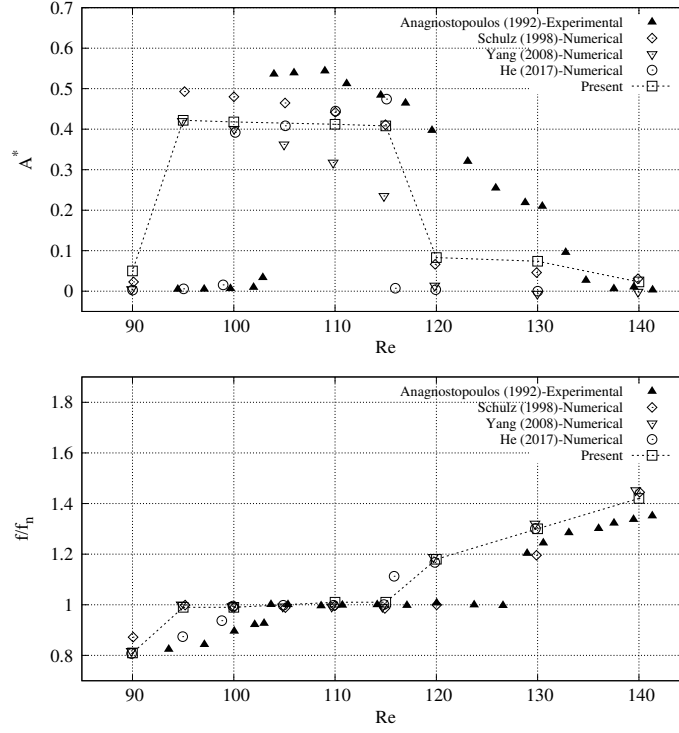
Figure 6: Amplitude of the cylinder vibration and vortex shedding frequency for different Reynolds numbers.

amplitude of the oscillations is significantly larger. The vortex shedding no longer occurs at the Strouhal frequency but in the natural structural frequency of the cylinder. The present numerical results are seen to agree fairly well with the experimental and other numerical data. The large vibration amplitudes in the lock-in region and the change of vortex shedding frequency to match the natural structural frequency of the cylinder are well captured. However, the maximum displacements are smaller than the experiments but in agreement with other numerical results. Moreover there is a slight shift in the lock-in region, i. e. the beginning and end of the numerical lock-in region occur at lower Reynolds numbers than their experimental counterparts. This shift happens for other numerical results as well [42, 43, 22]. The discrepancies may originate from the 3-D effects in the experiments that a 2-D simulation like this work can not capture. In the experimental study, the authors mention that no end plates were used on the cylinder [41]. Moreover the Reynolds numbers are close to the region of transition to 3-D (around

27

Re=180 for fixed cylinder). Thus it is possible that the Reynolds number locally exceeded the transition range and some 3-D effects were introduced to the flow.

Table 7 represents the VIV results obtained by the implicit, semi-implicit and semi-implicit-M coupling methods at Re=100. Results demonstrate that the accuracy of the proposed semi-implicit method is comparable to a fully implicit coupling technique. The discrepancies in maximum displacement, frequency and drag coefficient obtained by the semi-implicit method (with respect to implicit scheme) are 2.1%, 0.5% and 1.8% respectively. This clearly shows the capability of the proposed method in producing accurate results. Results of the modified version of the method, the semi-implicit-M, have a difference under 1% for all three parameters with respect to the implicit method. Again we see that implicit coupling of the dynamic mesh step (semi-implicit-M method) improves the accuracy of the results, however this improvement is not significant. This observation is similar to the previous test case where a slight improvement in the accuracy of the results were observed. This suggests that even in a FSI case with large deformations, explicit coupling of the dynamic mesh step does not noticeably reduce the accuracy of the results. This observation is also examined in the next test case with much larger structural deformations.

Table 7: Comparison of the VIV results obtained by different coupling methods at Re=100.

Coupling method	A^*	f/f_n	C_d
Implicit	0.427	0.993	1.62
Semi-implicit	0.418	0.988	1.59
Semi-implicit-M	0.424	0.990	1.60

Table 8 compares the performance of the implicit and semi-implicit coupling methods for the VIV case at Re=100. The performance criteria are the average number of coupling iterations and the overall CPU time of the simulations. All three coupling methods have been used with the same interface solver (FP-Aitken).

First thing to note in Table 8 is the much lower average number of iterations, comparing to the previous test case. While the previous test case required nearly 40 FSI coupling iterations per time step, the current problem only needs 2 or 3 iterations to converge. Since the density ratio for

28

Table 8: Performance comparison of implicit and semi-implicit coupling methods for VIV simulation at Re=100.

Coupling technique	Average No. of coupling iterations	Normalized CPU time
Implicit	3.2	2.9
Semi-implicit	2.1	1.0
Semi-implicit-M	3.0	2.6

the current test case is relatively large ($\rho_s/\rho_f = 149$), the added-mass effect is much smaller than the previous problem. Comparing Table 8 and Table 3 shows how strong added-mass effect makes a problem challenging in terms of stability and convergence. Because of the much smaller number of iterations, the CPU time ratio is also much smaller. The implicit method takes 2.9 times more CPU time (comparing to 12.9 times in the previous test case). Nevertheless, the superior performance of the semi-implicit method is still remarkable. It reduces the computational time by 65% with respect to the implicit method, while introducing a maximum of 2% error to the results. Again we see that the semi-implicit-M method noticeably increases the CPU time and its performance is not significantly better than the implicit scheme. Based on both test cases, we can conclude that implicit coupling of the dynamic mesh step only slightly improves the accuracy while significantly increasing the computational time.

Performance of different interface solvers for semi-implicit coupling method are compared in Table 9, using four criteria similar to the previous test case.

Table 9: Performance comparison of different interface solvers for semi-implicit coupling method for VIV case at Re=100.

Interface solver	Average No. of coupling iterations	No. of $\mathbf{S} \circ \mathbf{f}(\mathbf{d}_\Gamma)$ solutions per coupling iteration	Average No. of $\mathbf{S} \circ \mathbf{f}(\mathbf{d}_\Gamma)$ solutions per time step	Normalized CPU time
FP-Aitken	2.1	1	2.1	1.02
Newton-Krylov	1.4	1.1 (average)	1.5	1.00

As results in Table 9 show, the performance of the interface solvers are practically identical. The fixed-point method takes 2% more computational time which is negligible. This could be understood based on the low number of coupling iterations required for convergence in this test case. For such low number of iterations, a more advanced nonlinear interface solver (the Newton-Krylov method) does not have a practical advantage over a simpler fixed-point solver. Considering the simplicity of the FP-Aitken method, it is actually a better candidate for this class of FSI problems.

5.3. Driven cavity with a flexible bottom

A third test case is solved to further demonstrate the capability of the proposed method to stably solve FSI problems with large deformation of the solid boundary. The test case is a 2-D lid-driven cavity with a flexible bottom, as studied in [16, 8, 12]. The cavity is of a $1m \times 1m$ dimension. The top boundary of the cavity is moving with an oscillatory speed of $u(t) = 1 - cos(\omega t)$ with $\omega = 2\pi/5$. There are two openings of $0.1m$ length on the sidewalls that allow the fluid to enter to and exit from the domain. The openings are devised to make sure the incompressibility of the fluid does not constrain the structural deformation. Figure 7 shows a schematic description of the problem. The fluid density and viscosity are $\rho_f = 1.0kg/m^3$ and $\mu_f = 0.01Pa.s$, respectively. The flexible structure at the bottom has a thickness of $h = 0.05m$ and Young modulus $E = 250N/m^2$. The problem is solved for two different structural densities of $\rho_s = 50$ and $5kg/m^3$.

The flexible bottom is modeled as an Euler-Bernoulli beam, governed by the following equation:

$$\rho_s A \frac{\partial^2 \mathbf{d}}{\partial t^2} + EI \frac{\partial^4 \mathbf{d}}{\partial x^4} = q(x, t) \tag{42}$$

where $\mathbf{d} = [0, y, 0]^T$ in a Cartesian coordinate (x,y,z), A is the cross section area of the beam, I the second moment of area, and q is the load per unit length.

Structural governing equation is discretized in space using a finite-volume method along with a second-order central difference scheme. An implicit second-order finite difference scheme is used to discretize the second time derivative. A classical 31×31 grid is used to solve the problem. A 100×100 mesh was also used to solve one case with results changing less than 1%. A constant time step of $\Delta t = 0.001s$ is used for the simulations.
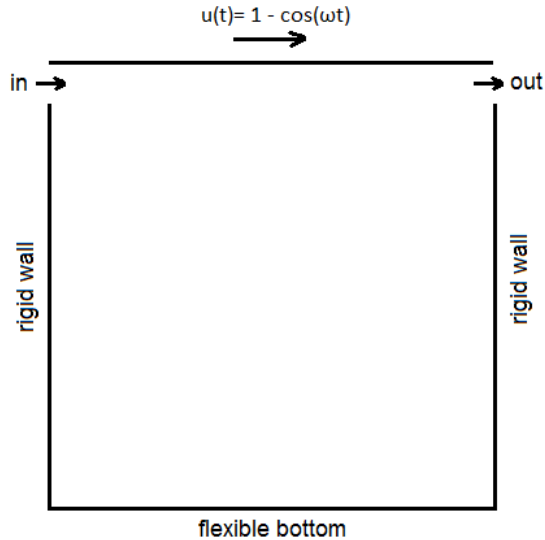
Figure 7: Schematic view of the problem setup for driven cavity with flexible bottom.

Figure 8 shows the fluid domain with structural deformation at the bottom, at $t = 19s$ (near maximum deflection) for the case with $\rho_s = 50kg/m^3$. Figure 9 and 10 compare the transient results obtained by the proposed semi-implicit method against a fully implicit coupling scheme. The results of the semi-implicit-M method are not shown in the figures for the sake of clarity of the pictures. As seen in the figures, the semi-implicit method provides an excellent accuracy with reference to an implicit method. The discrepancy for the case with $\rho_s = 50$ is very small (0.4% max). The semi-implicit-M method reduces the discrepancy marginally by 0.1%. For the case with $\rho_s = 5$, the semi-implicit method has a maximum of 2.5% error in the peak and trough points, with respect to the implicit method. The semi-implicit-M method reduces this discrepancy to 1.4%. It must be noted that the over-prediction at the peak points by the semi-implicit method does not indicate a stability problem. Although the peak values in Fig 10 are bigger for the semi-implicit method, the trough points are higher as well. It means the semi-implicit method does not amplify the oscillations artificially. The oscillation amplitude matches very well with that of the implicit method (0.5% max. discrepancy) and only the center line is slightly shifted upwards.
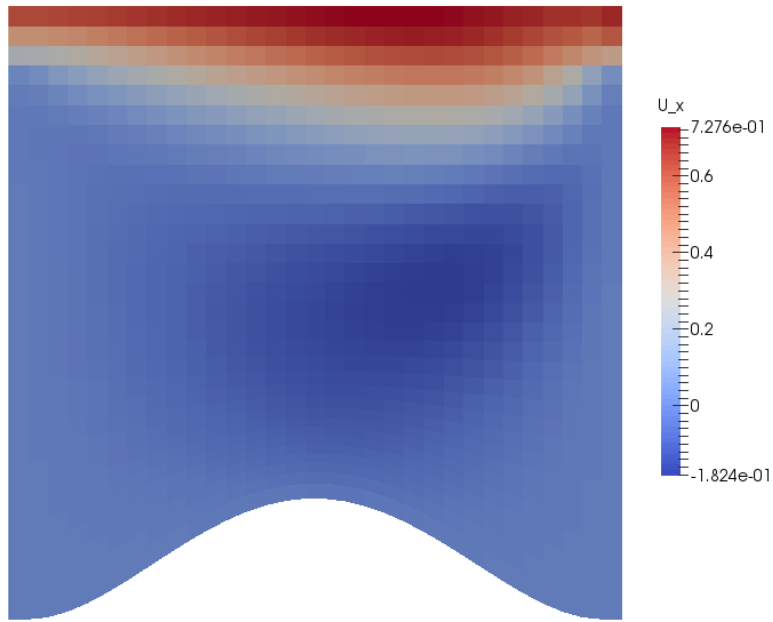
Figure 8: Flow field inside the cavity with deformed bottom, $t = 19s$, $\rho_s = 50 kg/m^3$.
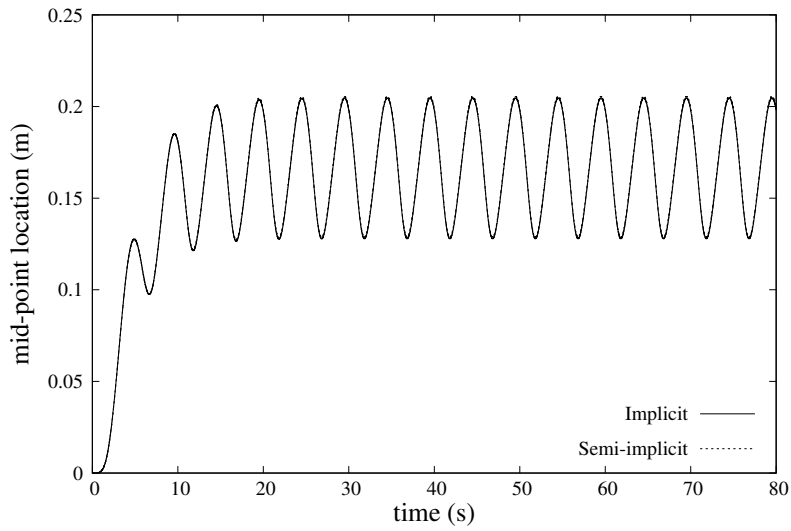

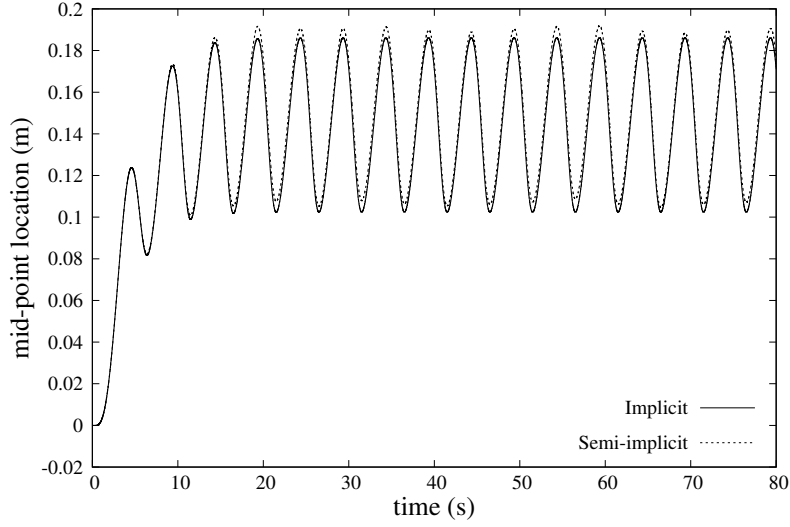Figure 9: Displacement of the mid-point of the structure over time, $\rho_S = 50 kg/m^3$.

Figure 10: Displacement of the mid-point of the structure over time, $\rho_S = 5kg/m^3$.

Table 10 contains the average number of coupling iterations and the overall solution time for each method, normalized by the smaller one. All three coupling methods have been used with the same interface solver (FP-Aitken). As results shows, the semi-implicit method is significantly cheaper than the fully implicit scheme, especially when higher number of coupling iterations are required. Again the semi-implicit-M method has a significantly higher CPU time compared to the semi-implicit method.

Table 10: Performance comparison of implicit and semi-implicit coupling methods for driven cavity with flexible bottom.

	Coupling technique	Average No. of coupling iterations	Normalized CPU time
	Implicit	2.5	2.2
$\rho_s = 50$	Semi-implicit	3.1	1.0
	Semi-implicit-M	2.6	2.0
	Implicit	7.8	5.9
$\rho_s = 5$	Semi-implicit	6.3	1.0
	Semi-implicit-M	6.1	4.2

The results of the third test case support the conclusions drawn in the previous sections. It shows that the semi-implicit method is capable of delivering a very good accuracy, compared to a fully implicit scheme. It also shows that implicit coupling of the dynamic mesh step (semi-implicit-M method) does not significantly improve the accuracy of the results, even for a case with large structural deformations. However, the semi-implicit-M method considerably increases the computational time.

6. Conclusion

A semi-implicit coupling method is proposed for fluid-structure interaction problems with strong added-mass effect. A fractional-step method is used to split the pressure stress term of the fluid and implicitly couple it to the structure. The remaining fluid terms are only explicitly coupled. An ALE formulation and conforming mesh technique is used to solve the fluid flow in a moving domain. A parallel radial basis function method is used to move the computational grid. The main advantages of the proposed method are:

- It is very simple, modular and completely matrix-free.

- Its robustness is tested in different FSI problems.

- It is computationally efficient.

Numerical tests are performed on three widely different test cases, which demonstrate adequate stability, accuracy and efficiency of the proposed method in different types of FSI problems, including ones with large deformations. Results of the simulations are validated against experimental data and other numerical results from the literature. A comparison is made between the accuracy and performance of the proposed semi-implicit method and a fully implicit coupling technique. Results show that the semi-implicit method significantly reduces the computational cost of the simulations without undermining either stability or accuracy of the results.

Moreover the effect of implicit or explicit coupling of the dynamic mesh step on overall performance and accuracy of the semi-implicit method is evaluated. Results show that implicit coupling of the dynamic mesh step remarkably increases the computational cost while only slightly improving the accuracy. This conclusion stands even for problems with large structural deformation.

Furthermore, we have used both fixed-point and Newton-Krylov methods to solve the interface problem. It is shown that the Newton-Krylov solver outperforms the fixed-point method in a problem that requires many iterations to converge. However, it also introduces extra complexity to the problem because of calculating the Jacobian. In a FSI problem which does not require many coupling iterations, fixed-point method with Aitken's relaxation is a better candidate, considering its simplicity and good performance.

7. Acknowledgements

8. References

[1] A. T. Barker, X.-C. Cai, Scalable parallel methods for monolithic coupling in fluid-structure interaction with application to blood flow modeling, Journal of Computational Physics 229 (3) (2010) 642–659. doi:10.1016/j.jcp.2009.10.001.

[2] A. Borghi, N. B. Wood, R. H. Mohiaddin, X. Y. Xu, Fluid-solid interaction simulation of flow and stress pattern in thoracoabdominal aneurysms: a patient-specific study, Journal of Fluids and Structures 24 (2) (2008) 270–280. doi:10.1016/j.jfluidstructs.2007.08.005.

[3] D. Shiels, A. Leonard, A. Roshko, Flow-induced vibration of a circular cylinder at limiting structural parameters, Journal of Fluids and Structures 15 (1) (2001) 3–21. doi:10.1006/jfls.2000.0330.

[4] P. Bearman, Circular cylinder wakes and vortex-induced vibrations, Journal of Fluids and Structures 27 (5) (2011) 648–658. doi:10.1016/j.jfluidstructs.2011.03.021.

[5] J. Degroote, Partitioned simulation of fluid-structure interaction, Archives of Computational Methods in Engineering 20 (2013) 185–238. doi:10.1007/s11831-013-9085-5.

[6] G. Hou, J. Wang, A. Layton, Numerical methods for fluid-structure interaction - A review, Communications in Computational Physics 12 (2) (2012) 337–377. doi:10.4208/cicp.291210.290411s.

[7] M. Lesoinne, C. Farhat, Higher-order subiteration-free staggered algorithm for nonlinear transient aeroelastic problems, AIAA Journal 36 (9) (1998) 1754–1757. doi:10.2514/2.7555.

[8] U. Küttler, W. a. Wall, Fixed-point fluid-structure interaction solvers with dynamic relaxation, Computational Mechanics 43 (2008) 61–72. doi:10.1007/s00466-008-0255-5.

[9] C. Michler, E. H. V. Brummelen, R. D. Borst, An interface Newton-Krylov solver for fuid-structure interaction, International Journal for Numerical Methods in Fluids 47 (10-11) (2005) 1189–1195. doi:10.1002/fld.850.

[10] M. A. Fernández, M. Moubachir, A Newton method using exact jacobians for solving fluid-structure coupling, Computers and Structures 83 (2005) 127–142. doi:10.1016/j.compstruc.2004.04.021.

[11] J. F. Gerbeau, M. Vidrascu, A quasi-Newton algorithm based on a reduced model for fluid-structure interaction problems in blood flows,

ESAIM: Mathematical Modelling and Numerical Analysis 37 (2003) 631–647. doi:10.1051/m2an:2003049.

[12] U. Kuttler, W. a. Wall, Vector extrapolation for strong coupling fluid-structure interaction solvers, Journal of Applied Mechanics 76 (2) (2009) 021205. doi:10.1115/1.3057468.

[13] C. Farhat, K. G. van der Zee, P. Geuzaine, Provably second-order time-accurate loosely-coupled solution algorithms for transient nonlinear computational aeroelasticity, Computer Methods in Applied Mechanics and Engineering 195 (2006) 1973–2001. doi:10.1016/j.cma.2004.11.031.

[14] E. Van Brummelen, Added mass effects of compressible and incompressible flows in fluid-structure interaction, Journal of Applied mechanics 76 (2) (2009) 021206. doi:10.1115/1.3059565.

[15] P. Causin, J. F. Gerbeau, F. Nobile, Added-mass effect in the design of partitioned algorithms for fluid-structure problems, Computer Methods in Applied Mechanics and Engineering 194 (2005) 4506–4527. doi:10.1016/j.cma.2004.12.005.

[16] C. Förster, W. a. Wall, E. Ramm, Artificial added mass instabilities in sequential staggered coupling of nonlinear structures and incompressible viscous flows, Computer Methods in Applied Mechanics and Engineering 196 (2007) 1278–1293. doi:10.1016/j.cma.2006.09.002.

[17] M. A. Fernández, J.-F. Gerbeau, C. Grandmont, A projection semi-implicit scheme for the coupling of an elastic structure with an incompressible fluid, International Journal for Numerical Methods in Engineering 69 (4) (2007) 794–821.

[18] M. Breuer, M. Münsch, Fluid-structure interaction using LES-A partitioned coupled predictor-corrector scheme, PAMM 8 (1) (2008) 10515–10516. doi:10.1002/pamm.200810515.

[19] M. Breuer, G. De Nayer, M. Münsch, T. Gallinger, R. Wüchner, Fluid-structure interaction using a partitioned semi-implicit predictor-corrector coupling scheme for the application of large-eddy simulation, Journal of Fluids and Structures 29 (2012) 107–130. doi:10.1016/j.jfluidstructs.2011.09.003.

[20] J. T. Grétarsson, N. Kwatra, R. Fedkiw, Numerically stable fluid–structure interactions between compressible flow and solid structures, Journal of Computational Physics 230 (8) (2011) 3062–3084. doi:10.1016/j.jcp.2011.01.005.

[21] M. Astorino, F. Chouly, M. A. Fernández, Robin based semi-implicit coupling in fluid-structure interaction: Stability analysis and numerics, SIAM Journal on Scientific Computing 31 (6) (2009) 4041–4065. doi:10.1137/090749694.

[22] T. He, K. Zhang, T. Wang, Ac-cbs-based partitioned semi-implicit coupling algorithm for fluid-structure interaction using stabilized second-order pressure scheme, Communications in Computational Physics 21 (5) (2017) 1449–1474. doi:10.4208/cicp.OA-2016-0106.

[23] I. González, O. Lehmkuhl, A. Naseri, J. Rigola, A. Oliva, Fluid-structure interaction of a reed type valve, in: International Compressor Engineering Conference, Purdue University Libraries, 2016, p. 2490.

[24] I. González, A. Naseri, J. Rigola, C. Pérez-Segarra, A. Oliva, A fluid-structure interaction solver for the fluid flow through reed type valves, in: IOP Conference Series: Materials Science and Engineering, Vol. 232, IOP Publishing, 2017, p. 012032.

[25] C. Hirt, A. A. Amsden, J. Cook, An arbitrary lagrangian-eulerian computing method for all flow speeds, Journal of computational physics 14 (3) (1974) 227–253. doi:10.1016/0021-9991(74)90051-5.

[26] J. Donea, S. Giuliani, J.-P. Halleux, An arbitrary lagrangian-eulerian finite element method for transient dynamic fluid-structure interactions, Computer methods in applied mechanics and engineering 33 (1-3) (1982) 689–723. doi:10.1016/0045-7825(82)90128-1.

[27] A. J. Chorin, Numerical solution of the Navier-Stokes equations, Mathematics of Computation 22 (1968) 745–762. doi:10.2307/2004575.

[28] R. Verstappen, A. Veldman, Symmetry-preserving discretization of turbulent flow, Journal of Computational Physics 187 (1) (2003) 343–368. doi:10.1016/S0021-9991(03)00126-8.

[29] L. Jofre, O. Lehmkuhl, J. Ventosa, F. X. Trias, A. Oliva, Conservation properties of unstructured finite-volume mesh schemes for the navier-stokes equations, Numerical Heat Transfer, Part B: Fundamentals 65 (1) (2014) 53–79. doi:10.1080/10407790.2013.836335.

[30] A. Gholami, D. Malhotra, H. Sundar, G. Biros, FFT, FMM, or multi-grid? A comparative study of state-of-the-art Poisson solvers for uniform and nonuniform grids in the unit cube, SIAM Journal on Scientific Computing 38 (3) (2016) C280–C306. doi:10.1137/15M1010798.

[31] F. X. Trias, O. Lehmkuhl, A. Oliva, C. D. Pérez-Segarra, R. W. C. P. Verstappen, Symmetry-preserving discretization of Navier-Stokes equations on collocated unstructured grids, Journal of Computational Physics 258 (2014) 246–267. doi:10.1016/j.jcp.2013.10.031.

[32] O. Estruch, O. Lehmkuhl, R. Borrell, C. D. P. Segarra, a. Oliva, A parallel radial basis function interpolation method for unstructured dynamic meshes, Computers and Fluids 80 (2013) 44–54. doi:10.1016/j.compfluid.2012.06.015.

[33] H. Wendland, Piecewise polynomial, positive definite and compactly supported radial functions of minimal degree, Advances in computational Mathematics 4 (1) (1995) 389–396. doi:10.1007/BF02123482.

[34] D. a. Knoll, D. E. Keyes, Jacobian-free Newton-Krylov methods: A survey of approaches and applications, Journal of Computational Physics 193 (2) (2004) 357–397. doi:10.1016/j.jcp.2003.08.010.

[35] Y. Saad, M. H. Schultz, GMRES: A Generalized Minimal Residual algorithm for solving nonsymmetric linear systems, SIAM Journal on Scientific and Statistical Computing 7 (3) (1986) 856–869. doi:10.1137/0907058.

[36] H. A. Van der Vorst, Bi-CGSTAB: A fast and smoothly converging variant of Bi-CG for the solution of nonsymmetric linear systems, SIAM Journal on scientific and Statistical Computing 13 (2) (1992) 631–644. doi:10.1137/0913035.

[37] S. C. Eisenstat, H. F. Walker, Choosing the forcing terms in an inexact Newton method, SIAM Journal on Scientific Computing 17 (1) (1996) 16–32. doi:10.1137/0917003.

[38] L. Formaggia, J. F. Gerbeau, F. Nobile, A. Quarteroni, On the coupling of 3D and 1D Navier-Stokes equations for flow problems in compliant vessels, Computer Methods in Applied Mechanics and Engineering 191 (6-7) (2001) 561–582. doi:10.1016/S0045-7825(01)00302-4.

[39] A. Quarteroni, M. Tuveri, A. Veneziani, Computational vascular fluid dynamics: Problems, models and methods, Computing and Visualization in Science 2 (2000) 163–197. doi:10.1007/s007910050039.

[40] A. Naseri, O. Lehmkuhl, I. Gonzalez, A. Oliva, Partitioned semi-implicit methods for simulation of biomechanical fluid-structure interaction problems, in: Journal of Physics: Conference Series, Vol. 745, IOP Publishing, 2016, p. 032020.

[41] P. Anagnostopoulos, P. Bearman, Response characteristics of a vortex-excited cylinder at low reynolds numbers, Journal of Fluids and Structures 6 (1) (1992) 39–50. doi:10.1016/0889-9746(92)90054-7.

[42] K. W. Schulz, Y. Kallinderis, Unsteady flow structure interaction for incompressible flows using deformable hybrid grids, Journal of Computational Physics 143 (2) (1998) 569–597. doi:10.1006/jcph.1998.5969.

[43] J. Yang, S. Preidikman, E. Balaras, A strongly coupled, embedded-boundary method for fluid–structure interactions of elastically mounted rigid bodies, Journal of Fluids and Structures 24 (2) (2008) 167–182. doi:10.1016/j.jfluidstructs.2007.08.002.